Journal of Materials Chemistry A

Accepted Manuscript

ROYAL SOCIETY OF CHEMISTRY

www.rsc.org/materialsA

Journal Name

ARTICLE

Toward high performance indacenodithiophene-based small-molecule organic solar cells: investigation of the effect of fused aromatic bridge on the device performance

Received 00th January 20xx,
Accepted 00th January 20xx

DOI: 10.1039/x0xx00000x

www.rsc.org/

Jin-Liang Wang,*[a][+] Fei Xiao,[a][+] Jun Yan,[b][+] Kai-Kai Liu,[a] Zheng-Feng Chang,[a] Ru-Bo Zhang,*[a] Hong-Bin Wu,*[b] and Yong Cao[b]

Here we report the synthesis of a pair of D_1-A-bridge-D_2-bridge-A-D_1 type small molecules **BIT4FDT** and **BIT4FTT.** Which have different π-conjugated bridges between indacenodithiophene (IDT) as electron-donating core and the electron-deficient difluorobenzothiadiazole unit and investigated the effects of π-conjugated bridges on their photovoltaic properties. We found the molecule **BIT4FTT**, containing thieno[3,2-b]thiophene which fused two thiophene rings as the π-conjugated bridges, exhibits different photophysical properties, the HOMO/LUMO energy level, charge carrier mobilities and the morphologies of blend films, and their photovoltaic properties, compared with the analogue system **BIT4FDT** which has 2,2'-bithiophene rings as the conjugated bridges. Moreover, both of two molecules devices after CH_2Cl_2 solvent annealing exhibited superior device performance than those of without CH_2Cl_2 solvent annealing. BHJ-OSC devices based on **BIT4FTT** and $PC_{71}BM$ increased from 5.85% to 7.57% (J_{sc} = 11.33 mA cm^{-2}, V_{oc} = 0.89 V, FF = 0.75) after exposure to CH_2Cl_2 vapor due to the obviously increase of both J_{sc} and FF. Interesting, the device based on **BIT4FDT** and **$PC_{71}BM$** give weaker response to solvent vapor annealing and much lower PCEs in comparison with these of **BIT4FTT**. The results indicate that the highly efficient small-molecules solar cells can be achieved using fused aromatic bridge and proper solvent vapor annealing process.

Introduction

Organic photovoltaic cells (OPVs) are considered to be one of the most promising candidates for the next generation energy sources because of their advantages such as light weight, flexibility, and low cost in recent years.[1] Over the past few years, extensive research efforts and significant progress have been made on bulk-heterojunction organic solar cells (BHJ-OSCs) based on donor/acceptor materials.[2] Recently, power conversion efficiencies (PCEs) over 10% have been achieved for single-junction solar cells based on π-conjugated polymers/fullerene derivatives.[3] However, some intrinsic disadvantages of polymers, such as less reproducibility, complex purification, and undefined relationship of structure and performance of final active materials, are still big challenges to further enhancement of device performances. Compared to polymer, small-molecules possess unique features of easy purification and well-defined discrete structure, which can ensure greater reproducibility in the device performance.[4] Furthermore, the small molecules could be viewed as model materials to simulate the backbone of high performance polymers, which is beneficial to investigate the relationships of structure-properties-device performance and disclose the key of the design of high performance photovoltaic materials. So far, significant progress has been made for solution processed small-molecule organic solar cells and notable PCE of over 9% has been achieved, which is catching the best-performance of polymer solar cells.[5] Most of the high PCE of small-molecule organic solar cells are based on benzodithiophene (BDT) core units,[6] dithienosilole (DTS) core unit,[7] porphyrin core units, and rhodanine derivative terminal group.[8] Using other building blocks, only moderate PCEs were obtained due to the poor film quality and low fill factor. Obviously, it is very important and challenge to develop high efficient novel conjugated small-molecules donor materials based on a next-generation core blocking unit with better film quality and high fill factor.

Recently, ladder-type indacenodithiophene (IDT) donor core has been applied into the small-molecular donor for BHJ-OSCs. However, most of these materials have exhibited relative lower fill factor due to the inferior intermolecular interaction and poor active layer morphology of these materials.[9] Meanwhile, incorporation of the fluorine atom into conjugated materials has become a popular strategy to improve the PCE

[a] Beijing Key Laboratory of Photoelectronic/Electrophotonic Conversion Materials, Beijing Institute of Technology, Beijing, 100081, China.
[b] Institute of Polymer Optoelectronic Materials and Devices, State Key Laboratory of Luminescent Materials and Devices, South China University of Technology, Guangzhou, 510640, China.
[+] These authors contributed equally to this work.
Electronic Supplementary Information (ESI) available: See DOI: 10.1039/x0xx00000x

relative to their fluorine-free analogue, which facilitated increase of open circuit voltage and formation of intramolecular hydrogen bonds to enhance of the intermolecular interaction.[10] In combination with the "fluorine (F) effect", we just reported **BIT-4F-T**, a linear small molecule containing thiophene functionalized IDT as the central donor unit, with two difluorobenzothiadiazole as the acceptor, which achieved excellent BHJ-OSCs performance with high FF.[11] These encouraging results indicated that difluorobenzothiadiazole/IDT-based small molecules become another novel family, high-efficiency, solution-processed, small-molecule donor materials. Thus, designing new materials by incorporating and/or modifying IDT unit might result in further advancement for small-molecule solar cells.

Meanwhile, it has been reported that the conjugation length and conjugated pattern of bridges between electron-donating group and electron-withdrawing wing group have significant impact on the photophysical properties, molecular packing, and charge carrier mobility of conjugated polymer and device performance.[12] For example, incorporating the fused ring thieno[3,2-b]-thiophene unit into conjugated polymers always enhance the π-electron delocalization and intermolecular interaction as well as reduce the energy bandgap in comparison with that of using the linear 2,2'-bithiophene unit.[13] Moreover, incorporating thieno[3,2-b]-thiophene groups functionalized difluorobenzothiadiazole unit into small molecule solar cells materials is really rare. Therefore, how the conjugation length and conjugated pattern of bridges of the small molecules affect their photophysical properties and device performance, particular before/after solvent vapour annealing or other post-treatments, need to be comprehensively investigated.

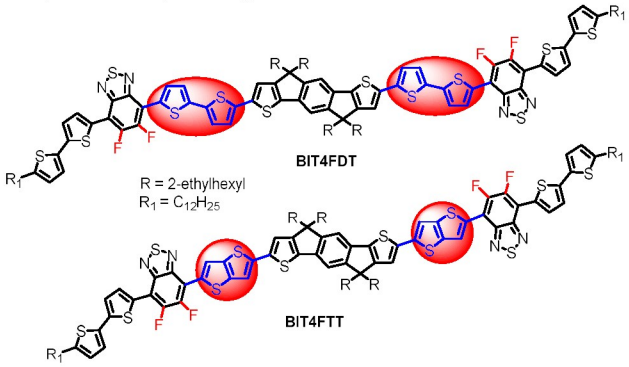

Chart 1. Chemical structures of **BIT4FDT** and **BIT4FTT.**

To address this challenge, in this work, two linear D_1-A-bridge-D_2-bridge-A-D_1 tetrafluorine substituted very similar small-molecules, namely as **BIT4FDT** and **BIT4FTT (Chart 1)** with the same electron-rich core (IDT as D_1), and electron-deficient unit (two difluorobenzothiadiazoles as A) and end groups (two *n*-dodecyls -substituted bithiophenes) but different π-conjugated bridge (2,2'-bithiophenes, thieno[3,2-b]-thiophene) between A unit and D_1 unit, were designed and synthesized. Although these two compounds have the similar backbone, we are wondering that the impact of the fusion or single bond connection of two thiophene in backbone structures. Therefore, we focused on whether the different of molecular rigidity and planarity of bithiophene and thieno[3,2-b]-thiophene as the bridge could affect the light-harvesting ability of the whole molecule, and the HOMO/LUMO energy level, charge carrier mobility, the morphologies of blend films, and their photovoltaic properties as electron donor material in the photoactive layer. These two materials both exhibit good solubility in common organic solvents such as $CHCl_3$, THF, toluene, and chlorobenzene owing to the multiple alkyl chains on IDT units and terminal thiophene groups and can be readily solution-processed and form excellent smooth films by spin-coating. In combination with using $PC_{71}BM$ as the acceptor, the BHJ-OSC devices based on **BIT4FTT** with an more rigidity and planarity π-conjugated backbone, exhibited better PCE of 7.57% with very-high FF of 0.75 for the device upon annealing by CH_2Cl_2 vapor for 30 s without using any additives. While the device based on **BIT4FDT** and **$PC_{71}BM$** give much lower PCEs in comparison with that of **BIT4FTT**. Moreover, these results provide a systematic investigation to understand the influence of the bridge unit in a series of conjugated D_1-A-bridge-D_2-bridge-A-D_1 small molecules by UV-vis absorption spectroscopy, atomic force microscopy, solvent vapor annealing process, device stability in air, transient photovoltage and photocurrent experiments and further correlate to the solar cells performances in this paper.

Results and discussion

The synthetic routes to these small molecules are shown in **Scheme 1**. **2** was obtained by a Stille coupling reaction between **1**[11] and 2-tributyltinthiophene in 90% isolated yield. Treatment of **2** with LDA followed by trimethyltin chloride and recrystallized from methanol/chloroform to afford the target product **3** as red solid. Treatment of **4**[14] with *N*-iodobutanimide in the mixture solvents of chloroform and AcOH to give dibromide **5** in high isolate yield. **BIT4FDT** with bithiopene as bridge was obtained through two-fold Stille coupling reaction between **3** and **5** in 61% isolated yield. **7** was prepared by a Stille coupling reaction between **6**[15] and 2-tributyltinthieno[3,2-b]-thiophene in isolated 83% yield, which was then converted to corresponding ditin **8** using *n*-BuLi and trimethyltin chloride. Finally, a Stille coupling reaction was carried out between **1** and **8** to give **BIT4FTT** in 71% isolated yield. All compounds were purified by silica gel column chromatography, and their structures and purity were full characterized by ^1H and ^{13}C NMR spectroscopy, elemental analysis, and ESI/MALDI-TOF MS. The thermal property of two small molecules was investigated by thermogravimetric analysis (**Figure 1**). Under N_2 atmosphere, the onset temperature with 5% weight-loss was about 416 °C for **BIT4FDT** and 407 °C for **BIT4FTT**, respectively, which indicated that the thermal stability of these small-molecules are stable enough for the studies of organic solar cells. Meanwhile, solid state thermal transitions were evaluated by using differential scanning calorimetry (DSC) under N_2 at a heating/cooling circle **(Figure S1)**. Upon the heating process, two molecules exhibit a clear melting temperatures (T_m), **BIT4FTT** exhibited obvious

higher melting points (about 255°C), which indicated that it has stronger intermolecular interaction than that of **BIT4FDT**.

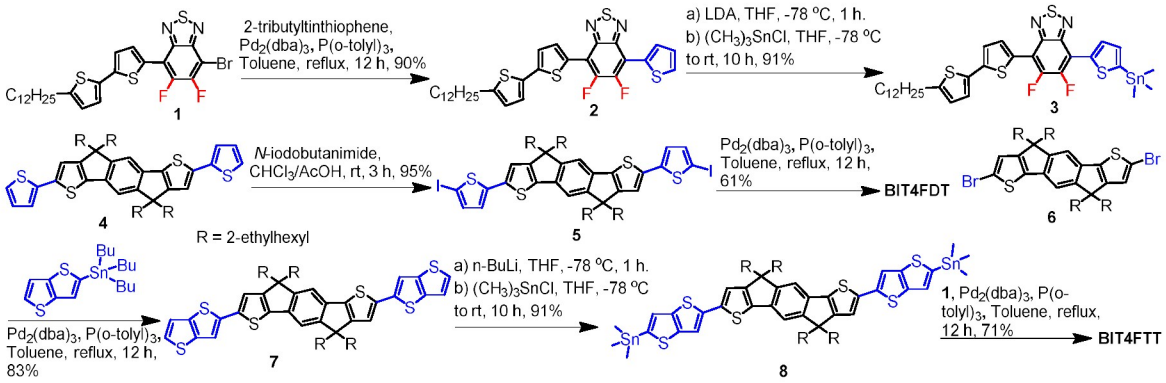

Scheme 1. The synthesis of **BIT4FDT** and **BIT4FTT.**

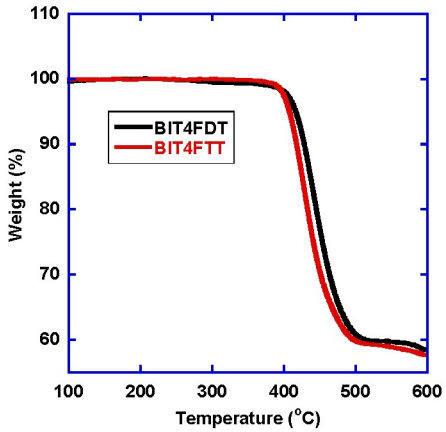

Figure 1. TGA of **BIT4FDT** and **BIT4FTT** with a heating rate of 10°C/min under N_2 atmosphere.

Figure 2 shows the absorption spectra of two small-molecules both in diluted chloroform solutions and in thin films, two molecules showed two distinct absorption bands (Band I: 300-500 nm; Band II: 500-800 nm) in solution and solid state due to π-π* transition of conjugated backbone and the intramolecular charge transfer (ICT) between molecular donor and acceptor unit. In solution, the small-molecule **BIT4FDT** shows an absorption peak at **470**nm and another more obvious absorption peak at **548** nm. the absorption peak of **BIT4FTT** based on thieno[3,2-b]-thiophene (TT) as bridge was located at about 567 nm and red-shifted about 19 nm in comparison with **BIT4FDT**, which might be attributed to the increase of molecular electron-donating ability and planarity from 2,2'-bithiophenes to thieno[3,2-b]-thiophene. Consequently, there should have more intense intermolecular π-π stacking interactions in **BIT4FTT** than **BIT4FDT**. The absorption spectra of two molecules in films are red-shifted and broader compared with their absorption spectra in solution. For example, compared with those absorption maximum peaks in solutions, **BIT4FTT** showed red-shift of 41 nm, while **BIT4FDT** red-shift only 12nm of λ_{max} peak in Band II region with a concomitant less intense peak at higher wavelengths in the solid state. The absorption spectra of **BIT4FTT** obviously increased the relative intensity of their 0-0 vibrational peak, which became as the maximum absorption peak. These results are probably due to the bigger conformation change, more efficient interchain interaction, and the higher π-electron delocalization of **BIT4FTT** than **BIT4FDT** in the solid states, which could be beneficial to a higher hole mobility and harvesting of solar irradiation. From the onset of absorption in thin films, the optical band gap of solid states were estimated to be 1.84 eV for **BIT4FDT** and 1.83 eV for **BIT4FTT**, respectively, as listed in **Table 1**.

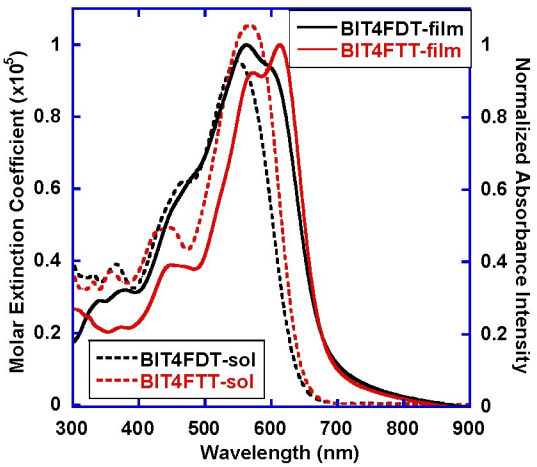

Figure 2. The absorption spectra of these small-molecules in chloroform solutions and in the thin films.

In order to investigate the relationship between the chemical structures and the electrochemical properties of the desired materials, the electrochemical properties of two small-molecules in thin films were investigated by cyclic voltammetry (CV). As shown in **Figure S3** and **Table 1**, the CV

curves of two materials both showed quasi-reversible oxidation and reduction waves. All potentials were recorded versus $Ag/AgNO_3$ (0.01 M in anhydrous acetonitrile) reference electrode and calibrated with the redox couple of Fc/Fc^+ under the same experimental conditions. The energy levels of the HOMO and LUMO are calculated according to the following equation of E_{HOMO} = -e(E_{Ox}+4.80) (eV) and E_{LUMO} = -e(E_{red}+4.80) (eV). As shown in **Table 1,** the HOMO levels of **BIT4FDT** and **BIT4FTT** both are located around -5.30 eV. While the LUMO energy levels of **BIT4FTT** are slight deeper relative to that of **BIT4FDT,** which is expected to gain the high J_{sc} of the resultant organic solar cells based **BIT4FTT**. The electrochemical band gaps ($E_{g(cv)}$) albeit slightly larger than the corresponding optical band gaps ($E_{g(opt)}$) because states measured in the electrochemical experiments (free ions) and that of the optical results (neutral states) are somewhat different.

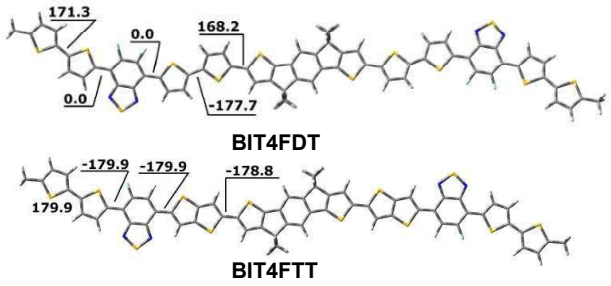

Figure 3. Comparison of optimized geometries of **BIT4FDT** and **BIT4FTT** using DFT B3LYP/6-31G(d) method.

Density functional theory (DFT) calculations were performed using B3LYP functional and 6-31G(d) basis sets to better understand the electronic structures geometry of **BIT4FDT** and **BIT4FTT.**[16] As shown **Figure 3**, Different π bridges between donor units and acceptor units can affect the molecular conformation. Due to the centrosymmetric of bithiophene and thieno[3,2-b]-thiophene bridges and the analysis of potential energy versus the torsional degree (see **Figure S4** and **S5**), both of **BIT4FDT** and **BIT4FTT** adapt the zigzag conformation as the lowest energy molecular conformation. While in the case of **BIT4FDT**, the dihedrals of bithiophene bridge as well as between the bridge and IDT are ca. 2.7° and 11.8°, which is obvious larger than **BIT4FTT**. Such non-coplanar feature would lead to less effective stacking of **BIT4FDT** in the solid state. As shown in **Table S2**, the computational results showed that **BIT4FDT** and **BIT4FTT** with the HOMO/LUMO energy levels were -4.68/-2.82, -4.68/ -2.83 respectively. The LUMO energy levels of **BIT4FTT** are deeper relative to that of **BIT4FDT,** which is consistent to the trend of electrochemical bandgaps.

To evaluate the potential of these small-molecules as promising electron donor materials in organic solar cells and understand the relationship of structure-properties-performance, we fabricated BHJ-OSCs with a device structure ITO/PEDOT:PSS (40 nm)/small-molecule:**$PC_{71}BM$** (90-100 nm)/PFN (5 nm)/Al (80 nm). The active layer was spin-coated from the blend solution at 50°C to gain high quality films. As an effective method for enhancement of PCE, solvent vapor annealing has been used in small molecule BHJ-OSCs to optimize the morphology of the active layer.[17] We further optimize the device performance of our small-molecules by using CH_2Cl_2 vapor annealing for 30 s without any additive. **Table 2** summarizes the device performance of two materials before and after solvent vapor annealing, such as V_{oc}, J_{sc}, FF, and PCE of the devices under 1 sun illumination.

The characteristic current density-voltage (*J*-V) curves for these optimal devices are shown in **Figure 4**. As expected, all of the devices based on our small-molecules and **$PC_{71}BM$** without solvent vapor treatment exhibited high V_{oc} due to the relative lower-lying HOMO energy levels of donor materials, for **BIT4FDT** and **BIT4FTT** were about 0.90 V and 0.93 V, respectively, which is associated with the wide bandgap characteristic. Moreover V_{oc} slightly decreased after solvent vapor annealing, which will be discussed later. Before solvent vapor annealing, the highest PCE of **BIT4FDT** and **BIT4FTT** were about 5.17% and 5.85% with **$PC_{71}BM$** by 1:3 ratios. There wasnot big difference between these two materials. While the overall performance of the devices from all of the donor materials were enhanced when CH_2Cl_2 vapor annealing treatment (30 s) was applied to the active layer, without the need of incorporation of additive. The best performance device based on **BIT4FTT:**$PC_{71}BM$ present the highest PCE of 7.57%, with a J_{sc} of 11.33 mA cm^{-2}, V_{oc} of 0.89 V, and a high FF of 0.75. It is have a large enhancement of PCE in comparison with the initial performance before CH_2Cl_2 vapor annealing. While the PCEs of the device based on **BIT4FDT:**$PC_{71}BM$ was enhanced in some extent (5.17% vs. 5.71%) after CH_2Cl_2 vapor annealing for 30 s due to large enhancing of FF with slight sacrificing of the J_{sc}. As shown in **Figure 4,** all of external quantum efficiencies (EQE) spectra covered a broad wavelength range from 300-800 nm for all the devices based on **BIT4FDT** and **BIT4FTT**. For **BIT4FTT** the conversion of photon to electrons is significantly improved from 400nm-650nm after exposure to CH_2Cl_2 vapor, which is consistent with the increase in J_{sc}. While the intensity of EQE spectra was obviously decreased in the entire photoactive region for **BIT4FDT** under CH_2Cl_2 vapor annealing which lead to decreased of J_{sc}. We also further examine the effect of other organic vapors (such as chloroform or THF) on solar cells performances. However, neither chloroform nor THF vapor annealing process can result in enhanced PCE due to significant decrease J_{sc} and V_{oc} (see **Table S2**) when compared to dichloromethane vapor annealing. For example, PCE of devices from **BIT4FTT/$PC_{71}BM$** blend after THF vapor annealing and after $CHCl_3$ vapor annealing were ~5.07% and ~4.05%, respectively. All the integrated current density from the EQE curve agrees well with the J_{sc} value from *J*-V curves.

To determine the origin of the observed photovoltaic performance differences between **BIT4FDT** and **BIT4FTT** as well as the effect of solvent vapor annealing on the active layer, we carried out more detailed investigations on blend absorption properties, morphology of blend films by atomic force microscopy (AFM), their charge mobility by space charge limited current (SCLC) method, device stability in air, transient photovoltage and photocurrent experiments to draw structure-property relationship.

Table 1. Photophysical and electrochemical properties of two small-molecules in solutions and in the thin films

Compd	λ_{max}abs. (sol) (nm)	λ_{max}abs. (film) (nm)	$E_{ox(onset)}$ (V) [a]	$E_{red(onset)}$ (V) [a]	E_{HOMO} (eV)	E_{LUMO} (eV)	$E_{g(cv)}$ (eV)	$E_{g(opt)}$ [b] (eV)
BIT4FDT	470, 548	562, 593 (sh)	0.50	-1.62	-5.30	-3.18	2.12	1.84
BIT4FTT	447, 567	567, 608	0.50	-1.60	-5.30	-3.20	2.10	1.83

[a] potentials are measured relative to a Fc/Fc^+ redox couple. [b] estimated from the onset of thin-film absorption.

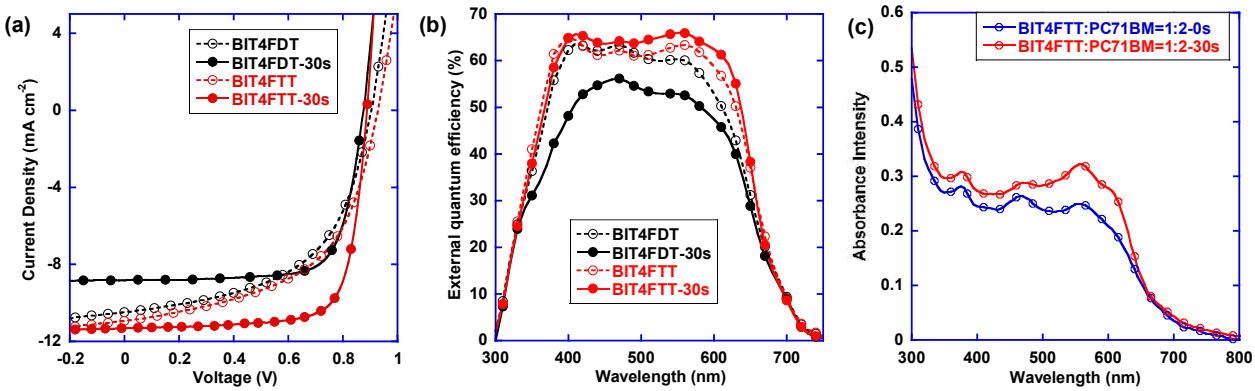

Figure 4. (a) Characteristic current density vs voltage (*J-V*) curves of the best OSC devices based on our small-molecules and **$PC_{71}BM$** before/after CH_2Cl_2 vapor annealing; (b) EQE curves of the best OSC devices based on our small-molecules and **$PC_{71}BM$** before/after CH_2Cl_2 vapor annealing; (c) Absorption spectra of **BIT4FTT/**$PC_{71}BM$ blend films before/after treatment with CH_2Cl_2 vapor annealing.

Table 2. A summary of the device performances of the organic solar cells and the charge carrier mobilities from blend films of two small-molecules and **$PC_{71}BM$** before/after CH_2Cl_2 vapor annealing.

Active layer	J_{sc} (mA/cm^2)	V_{oc} (V)	FF	PCE [b] (%)	μ_e (cm^{2}V^{-1}s^{-1})	μ_h (cm^{2}V^{-1}s^{-1})	μ_e/μ_h ratio
BIT4FDT/$PC_{71}BM$ (1:3)	10.49	0.90	0.55	5.17	2.1×10^{-4}	1.5×10^{-6}	14
BIT4FDT/$PC_{71}BM$ (1:3) [a]	8.83	0.88	0.73	5.71(5.55)	3.3×10^{-4}	1.0×10^{-4}	3.3
BIT4FDT/$PC_{71}BM$ (1:2)	7.66	0.90	0.55	3.82			
BIT4FDT/$PC_{71}BM$ (1:2) [a]	8.15	0.87	0.70	4.97			
BIT4FTT/$PC_{71}BM$ (1:3)	11.26	0.93	0.56	5.85			
BIT4FTT/$PC_{71}BM$ (1:3) [a]	11.16	0.88	0.73	7.20			
BIT4FTT/$PC_{71}BM$ (1:2)	10.93	0.93	0.54	5.85	2.3×10^{-4}	3.3×10^{-5}	7
BIT4FTT/$PC_{71}BM$ (1:2) [a]	11.33	0.89	0.75	7.57(7.50)	2.3×10^{-4}	2.3×10^{-4}	1

[a] treatment with CH_2Cl_2 vapor annealing for 30s. [b] the average PCEs are provided in parentheses

The origin of the obviously increased J_{sc} after CH_2Cl_2 vapor annealing for **BIT4FTT** was first investigated by the blend absorption spectra. As shown in **Figure 4**, compared to the absorption spectra of as-cast film, the spectra of the film with solvent vapor annealing showed enhanced absorption in 350-800 nm region, especially in range between 500 and700 nm. These more well-defined features across the entire visible spectrum and formation of a new vibronic shoulder at ca. 620 nm can be attributed to reorganization of **BIT4FTT** in the blend, as a result of a more ordered morphology, increase in molecular interaction and an enhancement in the absorption cross-section of the films. In the contrast, the blends for **BIT4FDT** has relative weaker influence, as indicated by the slight increase in intensity and absence of the obvious shoulder peak (see **Figure S6**). Therefore, the contribution from the increase of molecular interaction can be neglected, and it is not strange to see a decrease in J_{sc} after CH_2Cl_2 vapor annealing. Moreover, such results are consistent with the trend of EQE results of devices and will be discussed in details from the view of film morphology later.

Given the important role of film morphology of the active in determining the device performance of OSCs, we carried out tapping mode AFM study to reveal the morphology change upon the solvent annealing. The samples were prepared by spin-coating the donor: **$PC_{71}BM$** blend on ITO/PEDOT:PSS in the same way as the photoactive layers for the solar cell devices. As shown in **Figure 5,** without vapor annealing, the blend films based on **BIT4FDT** and **BIT4FTT** with **$PC_{71}BM$** were very smooth surface and uniform morphology with a small root-mean-square (RMS) roughness 1.2 nm for **BIT4FDT** and 0.5 nm for **BIT4FTT** respectively, indicating all of the donor materials have a good miscibility with $PC_{71}BM$. After CH_2Cl_2 vapor annealing for 30 s, the surface of the films based on **BIT4FDT** and **BIT4FTT/$PC_{71}BM$** become slightly rougher with RMS roughness of 1.6 nm and 0.9 nm in the same sequence as well as showed more phase-

separated and slightly bigger of domain size. Such features are in good agreement with the change of the blend films with/without solvent vapor annealing in the previous literature. We anticipated that CH_2Cl_2 vapor annealing can form a well interpenetrating network with a much rougher surface, which is consistent with feature of the absorption of the blend films upon CH_2Cl_2 vapor annealing. It can really increase in the domain and the more ordered film morphology of the active layer in nanoscale through the solvent vapor annealing, and thus preferable to improve charge transport properties.

Figure 6 shows the high-resolution TEM images of the blend films before and after the post solvent vapor annealing. Both of as-cast films exhibited homogeneous with inconspicuous phase-separated feature. In contrast, after CH_2Cl_2 vapor annealing, remarkable feature of phase separation and bicontinuous interpenetrating network could be clearly observed for both of the blend films. For example, phase-separated morphology with ca. 15-20 nm domain size for **BIT4FTT/PC$_{71}$BM** can be seen, which is beneficial for exciton dissociation at the D/A interface and charge transport along the interpenetrating network, thus is responsible for the increased J_{sc} and FF. On the other side, a larger domain size (ca. 25-30 nm) was found in **BIT4FDT/PC$_{71}$BM** film, which is away from the desired domain size for efficient diffusion. Nevertheless, the **BIT4FDT/PC$_{71}$BM** device after CH_2Cl_2 vapor annealing shows significant increase in FF, indicating the existence of a bicontinuous interpenetrating network, which is also very important for high performance of OPV devices.

The crystalline structures of **BIT4FTT/PC$_{71}$BM** blend films before/after CH_2Cl_2 vapor annealing were further characterized by X-ray diffraction (XRD) analysis. As shown in Figure S7, the as-cast blend films exhibited poor crystallinity with a weak (100) diffraction peak at about 4.5° and π-π stacking direction diffraction peak at about 22.5°. After the blend film was treated by CH_2Cl_2 vapor annealing, both diffraction peaks was enhanced obviously, which indicated that solvent vapor annealing treatment effectively promoted improvement of the order and crystallinity in the blend film.

To verify the positive effect of the CH_2Cl_2 vapor annealing on charge transporting and disclose their dependence on the structure of these two molecules, we compared the hole and electron mobility in the actual device before and after this treatment using a space charge limited current (SCLC) method. The structures of hole only and electron only device are ITO/PEDOT/small-molecules:PC$_{71}$BM/MoO_3/Al and ITO/ZnO/PFN/small-molecules: PC$_{71}$BM/Ca/Al, respectively. **Table 2** displays the hole and electron mobilities deduced from the SCLC method and **Figure S7-8** displays *J-V* characteristics of the hole-only and electron-only devices as obtained in dark. As expected, the devices based on **BIT4FDT** have the lower hole mobility (1.5×10^{-6} $cm^2V^{-1}s^{-1}$ and 1.0×10^{-4} $cm^2V^{-1}s^{-1}$) before/after CH_2Cl_2 vapor annealing due to the worst effective π-π stacking by having largest dihedrals in the structure as mentioned before. Moreover, the hole mobility for device fabricated from two small-molecule materials was enhanced about one order of magnitude after CH_2Cl_2 vapor annealing. For example, the hole mobility for original device fabricated from **BIT4FTT** is 3.3×10^{-5} $cm^2V^{-1}s^{-1}$. While it was enhanced to 2.3×10^{-4} $cm^2V^{-1}s^{-1}$ after treatment with CH_2Cl_2 vapor for 30 s. While the electron mobility (μ_e) of the original device fabricated from small-molecule/PC$_{71}$BM just increased slightly or unchanged. As a result, the imbalance of the hole and electron transport properties was dramatically improved after solvent vapor annealing. For **BIT4FTT**/PC$_{71}$BM, the μ_e/μ_h ratios dropped from 7.0 to 1.0, meanwhile for **BIT4FDT**/PC$_{71}$BM it dropped from 14 to 3.3 before and after CH_2Cl_2 vapor annealing for 30 s. Therefore, during CH_2Cl_2 vapor annealing process, the much enhanced μ_h together with considerably balanced hole and electron mobility of the device could result in a much higher charge-carrier extraction efficiency, which should account for their high FF. Actually, compared with the moderate FF (ca. 0.55) of small-molecule-based regular devices, all of the devices after CH_2Cl_2 vapor annealing for 30 s showed very high of FF (0.70-0.75), particular for **BIT4FTT** based devices, even up to 0.75, which should be associated with the best balanced charge carrier mobility and less charge recombination loss therein.[18]

To further examine the origin of the improved device performances by CH_2Cl_2 vapor annealing, we carried out transient photovoltage (TPV) and transient photocurrent (TPC) experiments to investigate the charge decay dynamics and determine the charge density in the devices based on **BIT4FDT** or **BIT4FTT** blend with **PC$_{71}$BM** with/without the CH_2Cl_2 vapor annealing under a give steady-state illumination.[19] For the TPV measurement, the perturbation from pulsed laser was attenuated by a set of neutral density filter so that the amplitude of TPV was much smaller as compared to V_{oc}. Since there was no charge collected under open-voltage condition, the excess charge carriers that excited by the pulsed laser were recombined inside the device. Therefore, the lifetime of the charge carriers could be extracted from the exponential fitting on the decay of the transient photovoltage. As shown in **Figure 7** and **Figure S9**, The extracted charge carrier lifetime (s) for two materials-based device before CH_2Cl_2 vapor annealing are similar (ca. 0.7 μs). However, after CH_2Cl_2 vapor annealing, the extracted charge carrier lifetime for **BIT4FDT**-based device was slightly increased to 1.5 μs, suggesting a reduced bimolecular recombination loss upon vapour annealing. For **BIT4FTT**-based device, the extracted charge carrier lifetime was unchanged. In conjunction with the slight increase or unchanged extracted charge carrier lifetime and the obviously increased hole mobility after CH_2Cl_2 vapor annealing, the exciton diffusion length at the D/A interface after CH_2Cl_2 vapor annealing is remarkable longer than that of the device without CH_2Cl_2 vapor annealing, which is responsible for the significant improvement in charge transport and FF after CH_2Cl_2 vapor annealing. Meanwhile, as revealed by the TPC measurement, upon CH_2Cl_2 vapor annealing, the charge carrier density slightly decreases in the **BIT4FDT** device while it increase in the **BIT4FTT** devices, which are in good agreement with the change of J_{sc} after vapor annealing (**Table 2**). In order to test the possibility of practical application, device shelf lifetime (storage stability) test was carried out in air environment after simple encapsulation. As shown in **Figure 8**, all of devices retained over 85% of initial PCE after about 150 h, which was obtained by counting the results from 8 individual cells of each type of small molecules and treatment conditions. Moreover, **BIT4FTT**-based device showed obviously better stability than those of **BIT4FDT**-based device. We believed that better device stability and lifetime could be achieved through an improved device architecture or proper encapsulation.

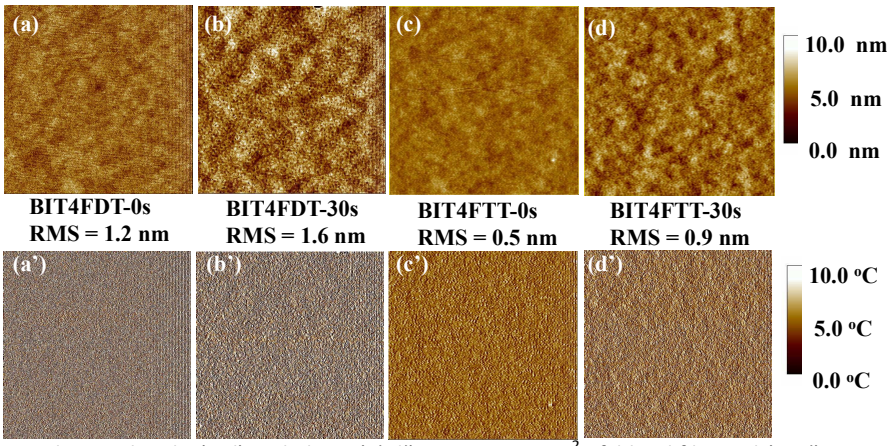

Figure 5. Tapping mode AFM height (a-d) and phase (a'-d') images 5×5 μm^2 of blend film with(a, a') **BIT4FDT/PC_{71}BM**; (b, b') **BIT4FDT/PC_{71}BM**after CH_2Cl_2 vapor annealing;(c, c') **BIT4FTT/PC_{71}BM**; (d, d') **BIT4FTT/PC_{71}BM**after CH_2Cl_2 vapor annealing.

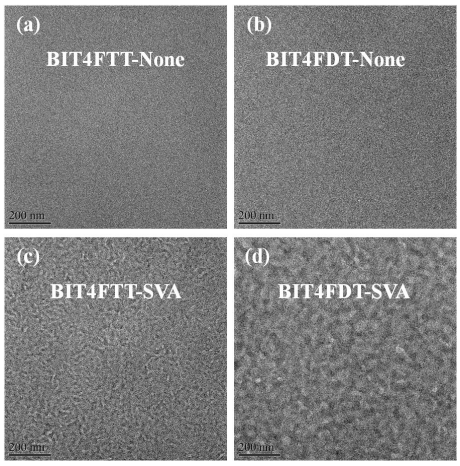

Figure 6. TEM images of blend films based on (a) **BIT4FTT**/PC_{71}BM; (b) **BIT4FDT**/PC_{71}BM; (c) **BIT4FTT**/PC_{71}BM after CH_2Cl_2 vapor annealing; (d) **BIT4FDT**/PC_{71}BM after CH_2Cl_2 vapor annealing. The scale bar is 200 nm.

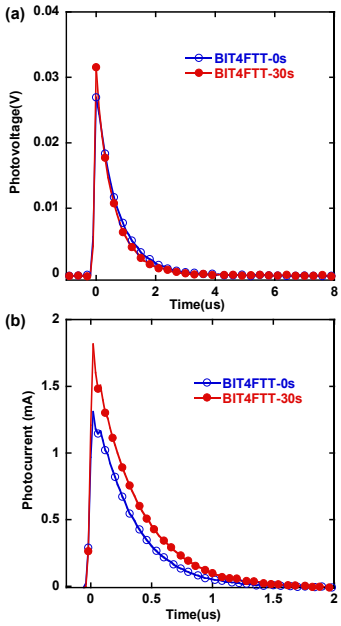

Figure 7. (a) Transient photovoltage and (b) Transient photocurrent for **BIT4FTT/PC_{71}BM** devices before and after CH_2Cl_2 vapor annealing, measured under 1 sun illumination and open-circuit voltage conditions using the same intensity laser pulse.

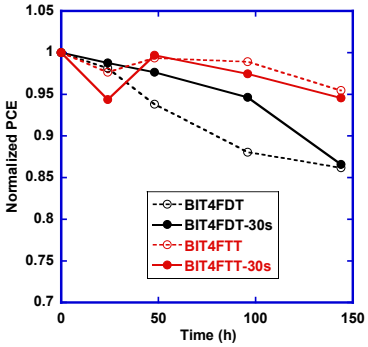

Figure 8. Stability curves of the devices based on these small molecules before and after CH_2Cl_2 vapor annealing for 30 s versus storage time in air.

Conclusions

In this study, we have designed and synthesized two linear tetrafluorine substituted small-molecules with the same IDT core, the same electron-deficient difluorobenzothiadiazole unit, and the same end groups but different conjugated pattern of bridge (single bond connection or fusion of two thiophene ring) for application in solution-processable organic solar cells. Although **BIT4FDT** and **BIT4FTT** have similar backbone, while **BIT4FTT** containing thieno[3,2-b] thiophene as the π-conjugated bridges, exhibits different photophysical properties, the HOMO/LUMO energy level, charge carrier mobilities and the morphologies of blend films, and their photovoltaic properties in comparison with the analogue system **BIT4FDT** with 2,2'-bithiophene rings as the conjugated bridges. The BHJ-OSC devices based on **BIT4FTT** and $PC_{71}BM$ show a significant improvement of the performance and exhibit the best PCE of ca. 7.6% with very-high FF of 0.75 upon annealing by CH_2Cl_2 for 30 s. These results indicated that CH_2Cl_2 vapor annealing is more effective for small molecule with fusion the π-bridge, which is easily to enhance the intermolecular interactions, the balance of charge carrier mobility and PCE. Throughout this study, it proves a valid strategy to combine the rotation design molecule through fusion π-bridge and device optimization to strike a suitable balance to achieve highly efficient organic photovoltaic devices.

Experimental Section

Materials and Characterization: All air and water sensitive reactions were performed under nitrogen atmosphere. Tetrahydrofuran (THF) was dried over Na/benzophenone ketyl and freshly distilled prior to use. The other materials were of the common commercial level and used as received. ^1H and ^{13}C NMR spectra were recorded on a Bruker ARX-400 (400 MHz) or ARX-500 (500 MHz) spectrometer, using $CDCl_3$, except where noted. All chemical shifts were reported in parts per million (ppm). ^1H NMR chemical shifts were referenced to TMS (0 ppm), and ^{13}C NMR chemical shifts were referenced to $CDCl_3$ (77.23 ppm). MALDI-TOF-MS was recorded on a Bruker BIFLEX III mass spectrometer. Thermal gravity analyses (TGA) were carried out on a TA Instrument Q600 analyzer. Elemental analyses were performed using a German Vario EL III elemental analyzer. Absorption spectra were recorded on PerkinElmer Lambda 750 UV-vis spectrometer. Cyclic voltammetry (CV) was performed on BASI Epsilon workstation. Glassy carbon electrode was used as a working electrode and a platinum wire as a counter electrode, these films were drop-cast on a glass carbon working electrode from THF solutions. Measurements were carried out at a scan rate of 50 mV/s in CH_3CN containing 0.1 M n-Bu_4NPF_6 as the supporting electrolyte. All potentials were calibrated with the redox couple of Fc/Fc^+ under the same experimental conditions. The film morphology was studied by atomic force microscopy (AFM, Veeco MultiMode V) operating in tapping mode.

BHJ-OSC fabrication. Device preparation and characterization were carried out in clean room conditions with protection against dust and moisture. The device structure was ITO/PEDOT:PSS/small-molecule:$PC_{71}BM$/PFN/Al, a 40-nm-thick PEDOT:PSS anode buffer layer was spin-cast on the ITO substrate, then dried in a vacuum oven at 100 ^oC overnight. The small-molecule:PC71BM active layer was prepared by spin-coating their mixture of chloroform and chlorobenzene solution with various weight ratios and then were placed in a glass petri dish containing 1 mL CH_2Cl_2 for 30 s for solvent vapor annealing. A 5 nm PFN layer was then spin-coated from methanol solution in presence of a trace amount of acetic acid onto the active layer. Subsequently, the films were transferred into a vacuum evaporator and 80 nm of Al were deposited as cathode. The active area of OPV devices is 0.16 cm^2 (~2×8 mm^2, as defined by a shadow mask).

2: In a 100 mL two-neck round-bottom flask, **1** (0.42 g, 0.72 mmol), 2-tributyltinthiophene (0.19 g, 1.44 mmol), $Pd_2(dba)_3$ (33 mg, 0.036 mmol), tri(*o*-tolyl)phosphine (44 mg, 0.14 mmol) was added. The flask was evacuated and back-filled with N_2 three times, and then degassed toluene (50 mL) was injected into the mixture. The resulting solution was stirred at room temperature for 12 h under the N_2 atmosphere. The solvents were then removed under reduced pressure. The dark residue was purified by silica gel chromatography, eluting with PE-CH_2Cl_2 (30:1) to give red solid (0.38 g, 90%). ^1H NMR ($CDCl_3$, 400 MHz, ppm): δ 8.28-8.29 (d, J = 3.6 Hz, 1H, Th-H), 8.20-8.21 (d, J = 3.6 Hz, 1H, Th-H), 7.60-7.62 (d, J = 4.8 Hz, 1H, Th-H), 7.26-7.27 (m, 1H, Th-H), 7.22-7.23 (d, J = 3.6 Hz, 1H, Th-H), 7.14-7.15 (d, J = 3.6 Hz, 1H, Th-H), 6.73-6.74 (d, J = 3.6 Hz, 1H, Th-H), 2.80-2.84 (t, J = 7.2 Hz, 2H, CH_2), 1.69-1.73 (m, 2H, CH_2), 1.26-1.40 (m, 18H, CH_2), 0.87-0.89 (t, J = 6.8 Hz, 3H, CH_3). ^{13}C NMR ($CDCl_3$, 100 MHz, ppm): δ (151.4, 153.2, 148.8, 148.6, J_{CF} = 258, 20 Hz), (151.2, 150.9, 148.6, 148.4, J_{CF} = 258, 20 Hz), (149.1, 148.8, J_{CF} = 22 Hz), 146.7, 141.7, 134.4, (132.07, 132.02, J_{CF} = 5 Hz), 131.9, 130.9, 129.9, 128.9, 127.6, 125.2, 124.3, 123.3, 111.8, 111.5, 32.2, 31.8, 30.5, 29.9, 29.8, 29.6, 29.4, 22.9, 14.3. HR-ESI-MS (*m/z*): calcd for $C_{30}H_{32}F_2N_2S_4$: 586.1416. Found: 586.1420 (M^+).

3: To a solution of **2** (0.29 g, 0.50 mmol) in anhydrous THF (50 mL) was added a solution of lithium diisopropylamide in THF (10 mL, 1.0 mmol) dropwise in N_2 atmosphere at -78 °C. The mixture was stirred at −78 °C for 1 h and Me_3SnCl (0.20 g, 1.0 mmol) in anhydrous THF (10 mL) was added. The mixture solution was warmed up to room temperature and stirred for 10 h. The mixture solution was quenched with water, and extracted with chloroform. The organic extracts were washed with brine and dried over anhydrous Na_2SO_4. After removal of the solvent under the reduced pressure, the resulting crude product was recrystallized from methanol and chloroform to afford the product as red solid (0.34 g, 91%).^1H NMR ($CDCl_3$, 400 MHz, ppm): δ 8.35 (m, 1H, Th-H), 8.20-8.21 (m, 1H, Th-H), 7.35 (m, 1H, Th-H), 7.24 (m, 1H, Th-H), 7.15 (m, 1H, Th-H), 6.74 (m, 1H, Th-H), 2.80-2.84 (t, J = 7.2 Hz, 2H, CH_2), 1.69-1.73 (m, 2H, CH_2), 1.27-1.40 (m, 18H, CH_2), 0.86-0.89 (t, J = 6.8 Hz, 3H, CH_3). 0.45 (s, 9H, CH_3). ^{13}C NMR ($CDCl_3$, 100 MHz, ppm): δ (151.3, 153.1, 148.7, 148.5, J_{CF} = 258, 20 Hz), (151.0, 150.8,

148.4, 148.2, J_{CF} = 258, 20 Hz), (149.2, 149.1, 148.9, 148.8, J_{CF} = 29, 9 Hz), 146.6, (142.83, 142.78, J_{CF} = 5 Hz), (141.5, 141.4, J_{CF} = 7 Hz), 137.3, 135.6, 134.5, (131.9, 131.8, J_{CF} = 10 Hz), (131.74, 131.66, J_{CF} = 8 Hz), 130.0, 125.2, 124.3, 123.3, (111.7, 111.5, 111.4, J_{CF} = 12 Hz), 32.2, 31.8, 30.5, 29.90, 29.88, 29.8, 29.60, 29.59, 29.4, 22.9, 14.3, -7.9. HR-ESI-MS (*m/z*): calcd for $C_{33}H_{40}F_2N_2S_4Sn$: 750.1064. Found: 750.1041 (M^+).

5: To a suspension of **4** (255 mg, 0.3 mmol) in $CHCl_3$ (15 mL) and AcOH (7mL) was added *N*-iodobutanimide (137 mg, 0.6 mmol).The resulting solution was stirred at room temperature for 3 h. The mixture solution was quenched with water, and extracted with chloroform. The organic extracts were washed with brine and dried over anhydrous Na_2SO_4. After removal of the solvents under the reduced pressure, the dark residue was purified by silica gel chromatography, eluting with PE to give yellow solid (311mg, 95%).^{1}H NMR ($CDCl_3$, 400 MHz, ppm): δ 7.26 (s, 2H, Ph-H), 7.16-7.17 (d, *J* = 3.6 Hz, 2H, Th-H), 7.00-7.01 (m, 2H, Th-H), 6.84-6.86 (m, 2H, Th-H), 1.93 (m, 8H, CH_2), 0.83-1.00 (m, 36H, CH_2), 0.50-0.74 (m, 24H, CH_2, CH_3). ^{13}C NMR ($CDCl_3$, 100 MHz, ppm): δ (155.72, 155.68, 155.64), 153.0, 144.8, (141.7, 141.64), 137.9, (137.12, 137.09), 135.8, (124.4, 124.32, 124.28), (119.85, 119.80), 114.2, 71.2, (54.19, 54.16), (44.1, 43.66), (35.22, 35.17, 35.14), (34.5, 34.4), (34.14, 34.10, 34.01, 33.97), (28.9, 28.8), 28.4, (27.6, 27.5, 27.4), (23.1, 23.0), (14.4, 14.3), (11.0, 10.8, 10.6). HR-ESI-MS (*m/z*): calcd for $C_{56}H_{76}I_2S_4$: 1130.2919. Found: 1130.2908 (M^+).

BIT4FDT: In a 100 mL two-neck round-bottom flask, **5** (0.23 g, 0.20 mmol), **3** (0.38 g, 0.50 mmol), and $Pd_2(dba)_3$ (9.2 mg, 0.01 mmol), tri(*o*-tolyl) phosphine (12.1 mg, 0.04 mmol) was added. The flask was evacuated and back-filled with N_2 three times, and then degassed toluene was injected into the mixture. The resulting solution was stirred at refluxing temperature for 12 h under the N_2 atmosphere. After being cooled to room temperature, the solvents were then removed under reduced pressure. The dark residue was purified by silica gel chromatography, eluting with PE-$CHCl_3$ (4:1) to give dark solid (0.25 g, 61%).^{1}H NMR ($CDCl_3$, 400 MHz, ppm): δ 8.23-8.24 (d, *J* = 3.6 Hz, 2H, Th-H), 8.21-8.22 (d, *J* = 3.6 Hz, 2H, Th-H), 7.32-7.33 (d, *J* = 3.6 Hz, 2H, Th-H), 7.30 (s, 2H, Ph-H), 7.27-7.28 (d, *J* = 3.6 Hz, 2H, Th-H), 7.24-7.25 (d, *J* = 3.6 Hz, 2H, Th-H), 7.15-7.16 (d, *J* = 3.6 Hz, 4H, Th-H), 7.13 (m, 2H, Th-H), 6.74-6.75 (d, *J* = 3.6 Hz, 2H, Th-H), 2.81-2.85 (t, *J* = 7.6 Hz, 4H, CH_2), 1.98 (m, 8H, CH_2), 1.69-1.73 (m, 4H, CH_2), 1.25-1.40 (m, 36H, CH_2), 0.88-1.04 (m, 40H, CH_2), 0.54-0.73 (m, 26H, CH_2, CH_3). ^{13}C NMR ($CDCl_3$, 100 MHz, ppm): δ 156.0, 153.2, 151.2, (151.0, 150.8, 148.9, 148.8, J_{CF} = 265, 21 Hz), 146.8, 141.8, 140.8, 138.8, 138.1, 136.0, 135.3, 134.5, (132.13, 132.05, J_{CF} = 10 Hz), 130.8, 130.1, (125.36, 125.30, J_{CF} = 8 Hz) 124.4, 124.0, 123.9, 123.5, 119.7, 114.2, (111.8, 111.7, J_{CF} = 12 Hz), (111.34, 111.25, J_{CF} = 11 Hz), 54.3, (44.5, 44.4, 44.0, 44.0), 35.4, (34.64, 34.55, 34.3, 34.2), 32.2, 31.8, 30.5, (29.9, 29.8), 29.6, 29.4, (29.1, 29.0), 28.5, (27.7, 27.6, 27.5, 27.4), (23.2, 23.1, 22.9), (14.4, 14.3), (11.0, 10.9, 10.6). MALDI-TOF MS (*m/z*): calcd for $C_{116}H_{138}F_4N_4S_{12}$: 2047.8 ($M^+$, 100%). Found: 2047.6 ($M^+$, 100%). Elemental Analysis: calcd for $C_{116}H_{138}F_4N_4S_{12}$: C, 67.99; H, 6.79; N, 2.73. Found: C, 68.18; H, 6.92; N, 2.61.

7: In a 100 mL two-neck round-bottom flask, **6** (870 mg, 1.0 mmol), 2-tributyltinthieno[3,2-b]-thiophene (1.08 g, 2.5 mmol), and $Pd_2(dba)_3$ (46 mg, 0.05 mmol), tri(*o*-tolyl)phosphine (61 mg, 0.2 mmol) was added. The flask was evacuated and back-filled with N_2 three times, and then degassed toluene was injected into the mixture. The resulting solution was stirred at refluxing temperature for 12 h under the N_2 atmosphere. After being cooled to room temperature, the solvents were then removed under reduced pressure. The dark residue was purified by silica gel chromatography, eluting with PE to give yellow oil (0.82 g, 83%).^{1}H NMR ($CDCl_3$, 400 MHz, ppm): δ 7.38 (s, 2H, Th-H), 7.34-7.36 (d, *J* = 4.8 Hz, 2H, Th-H), 7.31 (s, 2H, Ph-H), 7.23-7.24 (d, *J* = 4.8 Hz, 2H, Th-H), 7.12 (m, 2H, Th-H), 1.99 (m, 8H, CH_2), 0.88-1.04 (m, 36H, CH_2), 0.55-0.75 (m, 24H, CH_2, CH_3), ^{13}C NMR ($CDCl_3$, 100 MHz, ppm): δ (155.77, 155.68), 153.0, (141.63, 141.60), 140.8, 140.1, (138.64, 138.61), 137.8, 135.9, 127.0, 119.7, (119.65, 119.56), 115.0, 114.2, 54.22, (44.3, 43.7), (35.3, 35.22, 35.19, 35.14), (34.5, 34.4), (34.21, 34.17), (34.08, 34.05), 28.9, 28.8, (28.45, 28.43, 28.40), (27.6, 27.5, 27.3), (23.1, 23.03, 23.01), (14.4, 14.3), 11.0, 10.8, 10.63. HR-ESI-MS (*m/z*): calcd for $C_{60}H_{78}S_6$: 990.4428. Found: 990.4402 (M^+).

8: To a solution of **7** (0.25 g, 0.25 mmol) in anhydrous THF (50 mL) was added a solution of *n*-BuLi in hexane (0.3 mL, 0.65 mmol) dropwise in N_2 atmosphere at −78 °C. The mixture was stirred at −78 °C for 1 h and Me_3SnCl (0.15 g, 0.75 mmol) in anhydrous THF (10 mL) was added. The mixture solution was warmed up to room temperature and stirred for 10 h. The mixture solution was quenched with water, and extracted with chloroform. The organic extracts were washed with brine and dried over anhydrous Na_2SO_4. After removal of the solvents under the reduced pressure, the product was obtained as yellow oil (0.30 g, 91%) and used in the next step without any further purification. ^{1}H NMR ($CDCl_3$, 400 MHz, ppm): δ 7.34 (s, 2H, Th-H), 7.27 (s, 2H, Ph-H), 7.26 (m, 2H, Th-H), 7.09 (m, 2H, Th-H), 1.96 (m, 8H, CH_2), 0.91-0.95 (m, 36H, CH_2), 0.52-0.72 (m, 24H, CH_2, CH_3), 0.42 (s, 18H, CH_3). ^{13}C NMR ($CDCl_3$, 100 MHz, ppm): δ (155.68, 155.63, 155.60), 152.9, 145.7, (141.4, 141.28), 140.6, 139.7, 138.9, 135.9, 126.7, (119.43, 119.38, 119.32), (114.6, 114.1), (54.20, 54.18), (44.3, 43.7), (35.17, 35.14), (34.5, 34.4), (34.19, 34.15, 34.06, 34.02), (28.9, 28.8), 28.4, (27.6, 27.5, 27.3), (23.1, 23.00), (14.4, 14.3), (11.0, 10.8, 10.63), -7.9. HR-ESI-MS (*m/z*): calcd for $C_{66}H_{94}S_6Sn_2$: 1318.3724. Found: 1318.3694 (M^+).

BIT4FTT: In a 100 mL two-neck round-bottom flask, **8** (0.20 g, 0.15 mmol), **1** (0.19 g, 0.38 mmol), and $Pd_2(dba)_3$ (6.9 mg, 0.0075 mmol), tri(*o*-tolyl)phosphine (9.1 mg, 0.03 mmol) was added. The flask was evacuated and back-filled with N_2 three times, and then degassed toluene was injected into the mixture. The resulting solution was stirred at refluxing temperature for 12 h under the N_2 atmosphere. After being cooled to room temperature, the solvents were then removed under reduced pressure. The dark residue was purified by silica gel chromatography, eluting with PE-$CHCl_3$ (4:1) to give dark solid (0.21 g, 71%). ^{1}H NMR ($CDCl_3$, 400 MHz,

ppm): δ 8.55 (s, 2H, Th-H), 8.22-8.23 (d, *J* = 3.6 Hz, 2H, Th-H), 7.44 (s, 2H, Th-H), 7.34 (s, 2H, Ph-H), 7.24-7.25 (d, *J* = 3.6 Hz, 2H, Th-H), 7.19-7.20 (m, 2H, Th-H), 7.16-7.17 (d, *J* = 3.6 Hz, 2H, Th-H), 6.74-6.75 (d, *J* = 3.6 Hz, 2H, Th-H), 2.81-2.85 (t, *J* = 7.6 Hz, 4H, CH_2), 2.00 (m, 8H, CH_2), 1.70-1.73 (m, 4H, CH_2), 1.27-1.40 (m, 36H, CH_2), 0.88-1.05 (m, 40H, CH_2), 0.58-0.75 (m, 26H, CH_2, CH_3). ^{13}C NMR ($CDCl_3$, 100 MHz, ppm): δ 156.0, 153.2, (151.4, 151.2, 148.8, 148.6, J_{CF} = 258, 20 Hz), 151.1, (149.0, 148.9, J_{CF} = 10 Hz), 146.8, 143.3, 142.8, 142.3, 141.8, 138.5, 138.3, 136.0, 134.4, 133.4, (132.14, 132.05, J_{CF} = 10 Hz), 130.0, 125.3, 124.4, 123.5, 123.3, 120.0, 114.8, 114.3, 111.7, 54.3, (44.4, 43.9), 35.3, 34.5, (34.2, 34.1), 32.2, 31.8, 30.5, 29.9, 29.8, 29.6, 29.4, 29.0, 28.9, 28.5, 27.5, 23.1, 22.9, 14.35, 11.0, 10.9, 10.7. MALDI-TOF MS (*m/z*): calcd for $C_{112}H_{134}F_4N_4S_{12}$: 1995.7 ($M^+$, 100%). Found: 1996.8 ($[M+1]^+$, 100%). Elemental Analysis: calcd for $C_{112}H_{134}F_4N_4S_{12}$: C, 67.36; H, 6.76; N, 2.81. Found: C, 67.69; H, 6.80; N, 2.77.

Acknowledgements

This work was financially supported by the grants from the National Natural Science Foundation of China (21472012, 21202007, 51225301, 91333206); the Thousand Youth Talents Plan of China; Beijing Natural Science Foundation (2152027). The Development Program for Distinguished Young and Middle-aged Teachers and Special programs to cultivate major projects of Beijing Institute of Technology.

Notes and references

1 (a) P. M. Beaujuge and J. M. J. Fréchet, *J. Am. Chem. Soc.* 2011, **133**, 20009-20029; (b) G. Dennler, M. C. Scharber and C. J. Brabec, *Adv. Mater.* 2009, **21**, 1323-1328; (c) O. Inganäs, F. Zhang and M. R. Andersson, *Acc. Chem. Res.* 2009, **42**, 1731-1739; (d) Y. Li, *Acc. Chem. Res.* 2012, **45**, 723-733; (e) H. Zhou, L. Yang and W. You, *Macromolecules*, 2012, **45**, 607-632; (f) L. Ye, S. Zhang, L. Huo, M. Zhang and J. Hou, *Acc. Chem. Res.* 2014, **47**, 1595-1603; (g) H.-Y. Chen, J. Hou, S. Zhang, Y. Liang, G. Yang, Y. Yang, L. Yu, Y. Wu and G. Li, *Nat. Photon.* 2009, **3**, 649-653.

2 (a) S. Price, A. Stuart, L. Yang, H. Zhou and W. You, *J. Am. Chem. Soc.* 2011, **133,** 4625-4631; (b) X. Guo, N. Zhou, S. J. Lou, J. W. Hennek, R. P. Ortiz, M. R. Butler, P.-L. Boudreault, J. Strzalka, P.-O. Morin, M. Leclerc, J. T. L. Navarrete, M. A. Ratner, L. X. Chen, R. P. H. Chang, A. Facchetti and T. J. Marks, *J. Am. Chem. Soc.* 2012, **134**, 18427-18439; (c) C. Cabanetos, A. E. Labban, J. A. Bartelt, J. D. Douglas, W. R. Mateker, J. M. J. Fréchet, M. D. McGehee and P. M. Beaujuge, *J. Am. Chem. Soc.* 2013, **135**, 4656-4659; (d) I. Osaka, T. Kakara, N. Takemura, T. Koganezawa and K. Takimiya, *J. Am. Chem. Soc.* 2013, **135**, 8834-8344; (e) K. Li, Z. Li, K. Feng, X. Xu, L. Wang and Q. Peng, *J. Am. Chem. Soc.* 2013, **135**, 13549-13557; (f) W. Li, K. H. Hendriks, A. Furlan, M. M. Wienk and R. A. J. Janssen, *J. Am. Chem. Soc.* 2015, **137**, 2231-2234.

3 (a) Z. He, B. Xiao, F. Liu, H. Wu, Y. Yang, S. Xiao, C. Wang, T. P. Russell and Y. Cao, *Nat. Photon.* 2015, **9**, 174-179; (b) J.-D. Chen, C. Cui, Y.-Q. Li, L. Zhou, Q.-D. Ou, Li, C.; Y. Li and J.-X. Tang, *Adv. Mater.,* 2015, **27**, 10135; (c) Y. Liu, J. Zhao, Z. Li, C. Mu, W. Ma, H. Hu, K. Jiang, H. Lin, H. Ade and H. Yan, *Nat. Commun*. 2014, **5**, 5293; (d) L. Ye,; S. Zhang, W. Zhao, H. Yao and J. Hou, *Chem. Mater.*, 2014, **26**, 3603-3605; (e) T. L. Nguyen, H. Choi, S.-J. Ko, M. A. Uddin, B. Walker, S. Yum, J.-E. Jeong, M. H. Yun, T. J. Shin, S. Hwang, J. Y. Kim and H. Y. Woo, *Energy Environ. Sci.* 2014, **7**, 3040-3051; (f) L. Huo, T. Liu, X. Sun, Y. Cai, A. J. Heeger and Y. Sun, *Adv. Mater.* 2015, **27**, 2938-2944; (j) J. Zhang, Y. Zhang, J. Fang, K. Lu, Z. Wang, W. Ma and Z. Wei, *J. Am. Chem. Soc.* 2015, **137**, 8176-8183;(h) J. Cao, L. Qian, F. Lu, J. Zhang, Y. Feng, X. Qiu, H.-L. Yip and L. Ding, *Chem. Commun.* 2015, **51**, 11830-11833; (i) L. Huo, T. Liu, B. Fan, Z. Zhao, X. Sun, D. Wei, M. Yu, Y. Liu and Y. Sun, *Adv. Mater.* 2015, **27**, 6969.

4 (a) A. Mishra and P. Bauerle, *Angew. Chem. Int. Ed.* 2012, **51**, 2020-2067; (b) Y. Lin, Y. Li and X. Zhan, *Chem. Soc. Rev.* 2012, **41**, 4245-4272; (c) Y. Chen, X. Wan and G. Long, *Acc. Chem. Res.* 2013, **46**, 2645-2655; (d) J. E. Coughlin, Z. B. Henson, G. C. Welch and G. C. Bazan, *Acc. Chem. Res.* 2014, **47**, 257-270; (e) J. Roncali, P. Leriche and P. Blanchard, *Adv. Mater.* 2014, **26**, 3821-3838.

5 (a) W. Ni, X. Wan, M. Li, Y. Wang and Y. Chen, *Chem. Commun.* 2015, **51**, 4936-4950; (b) Y. Lin, Z.-G. Zhang, H. Bai, J. Wang, Y. Yao, Y. Li, D. Zhu and X. Zhan, *Energy Environ. Sci*., 2015, **8**, 610-616; (c) C. Cui, X. Guo, J. Min, B. Guo, X. Cheng, M. Zhang, C. J. Brabec and Y. Li, *Adv. Mater.* DOI:10.1002/adma.201503815; (d) N. Lim, N. Cho, S. Paek, C. Kim, J. K. Lee and J. Ko, *Chem. Mater.* 2014, **26**, 2283-2288; (e) H. Gao, Y. Li, L. Wang, C. Ji, Y. Wang, W. Tian, X. Yang and L. Yin, *Chem. Commun.* 2014, **50**, 10251-10254; (f) M. Moon, B. Walker, J. Lee, S. Y. Park, H. Ahn, T. Kim, T. Lee, H. Heo, J. J. H Seo, T. J. Shin, J. Y. Kim and C. Yang, *Adv. Energy. Mater.* 2015, **5**, 1402044; (j) A. Tang, C. Zhan and J. Yao, *Chem. Mater.* 2015, **27**, 4719-4730; (h) M. Cheng, C. Chen, X. Yang, J. Huang, F. Zhang, B. Xu and L. Sun, *Chem. Mater.* 2015, **27**, 2808-1814; (i) V. S. Gevaerts, E. M. Herzig, M. Kirkus, K. H. Hendriks, M. M. Wienk, J. Perlich, P. Müller-Buschbaum and R. A. J. Janssen, *Chem. Mater.* 2014, **26**, 916-926; (j) J.-L. Wang, Z. Wu, J.-S. Miao, K.-K. Liu, Z.-F. Chang, R.-B. Zhang, H.-B. Wu and Y. Cao, *Chem. Mater.* 2015, **27**, 4338−4348; (k) D. Yang, Y. Jiao, L. Yang, Y. Chen, S. Mizoi, Y. Huang, X. Pu, Z. Lu, H. Sasabe and J. Kido, *J. Mater. Chem. A.* 2015, **3**, 17704-17712. (l) J.-L. Wang, F. Xiao, J. Yan, Z. Wu, K.-K. Liu, Z.-F. Chang, R.-B. Zhang, H. Chen, H.-B. Wu and Y. Cao, *Adv. Funct. Mater.* 2015, 10.1002/adfm.201505020.

6 (a) J. Zhou, Y. Zuo, X. Wan, G. Long, Q. Zhang, W. Ni, Y. Liu, Z. Li, G. He, C. Li, B. Kan, M. Li and Y. Chen, *J. Am. Chem. Soc.* 2013, **135**, 8484-8487; (b) B. Kan, Q. Zhang, M. Li, X. Wan, W. Ni, G. Long, Y. Wang, X. Yang, H. Feng and Y. Chen, *J. Am. Chem. Soc.* 2014, **136**, 15529-15532; (c) B. Kan, M. Li, Q. Zhang, F. Liu, X. Wan, Y. Wang, W. Ni, G. Long, X. Yang, H. Feng, Y. Zuo, M. Zhang, F. Huang, Y. Cao, T. P. Russell and Y. Chen, *J. Am. Chem. Soc.* 2015, **137**, 3886-3893; (d) L. Yuan, Y. Zhao, J. Zhang, Y. Zhang, L. Zhu, K. Lu, W. Yan and Z. Wei, *Adv. Mater.* 2015, **27**, 4229-4233.

7 (a) Y. Sun, G. C. Welch, W. L. Leong, C. J. Takacs, G. C. Bazan and A. J. Heeger, *Nat. Mater.* 2012**, 11***,* 44-48; (b) J. A. Love, I. Nagao, Y. Huang, M. Kuik, V. Gupta, C. J. Takacs, J. E. Coughlin, L. Qi, T. S. van der Poll, E. J. Kramer, A. J. Heeger, T.-Q. Nguyen and G. C. Bazan, *J. Am. Chem. Soc.* 2014**, 136**, 3597-3606; (c) A. K. K. Kyaw, D. H. Wang, D. Wynands, J. Zhang, T.-Q. Nguyen, G. C. Bazan and A. J. Heeger, *Nano. Lett.* 2013**, 13**, 3796-3801.

8 (a) H. Qin, L. Li, F. Guo, S. Su, J. Peng, Y. Cao and X. Peng, *Energy Environ. Sci.* 2014, **7**, 1397-1401;(b) K. Gao, L. Li, T. Lai, L. Xiao, Y. Huang, F. Huang, J. Peng, Y. Cao, F. Liu, T. P. Russell, R. A. J. Janssen and X. Peng, *J. Am. Chem. Soc.* 2015, **137**, 7282-7285.

9 (a) J. J. Intemnan, K. Yao, F. Ding, Y. Xu, X. Xin, X. Li and A. K.-Y. Jen, A*dv. Funct. Mater.* 2015, **25**, 4889-4897; (b) H. Bai, Y. Wang, P. Cheng, Y. Li, D. Zhu and X. Zhan, *ACS Appl.*

Mater. Interfaces, 2014, **6**, 8426-8433; (c) D. Liu, M. Xiao, Z. Du, Y. Yan, L. Han, V. A. L. Roy, M. Sun, W. Zhu, C. S. Lee and R. Yang, *J. Mater. Chem. C,* 2014, **2**, 7523-7530.

10 (a) J. H. Park, E. H. Jung, J. W. Jung and W. H. Jo, *Adv. Mater.* 2013, **25**, 2583-2588; (b) W. Li, S. Albrecht, L. Yang, S. Roland, J. R. Tumbleston, T. McAfee, L. Yan, M. A. Kelly, H. Ade, D. Neher and W. You, *J. Am. Chem. Soc.* 2014, **136**, 15566-15576; (c) S. Yum, T. K. An, X. Wang, W. Lee, M. A. Uddin, Y. J. Kim, T. L. Xu, S. Nguyen, S. Hwang, C. E. Park and H. Y. Woo, *Chem. Mater.* 2014, **26**, 2147-2154; (d) M. Zhang, X. Guo, S. Zhang, J. Hou, *Adv. Mater.* 2014, **26**, 1118-1123.

11 J.-L.Wang, Q.-R. Yin, J.-S. Miao, Z. Wu, Z.-F. Chang, Y. Cao, R.-B. Zhang, J.-Y. Wang, H.-B. Wu and Y. Cao, *Adv. Funct. Mater.* 2015, **25**, 3514–3523.

12 (a) H. Feng, M. Li, W. Ni, F. Liu, X. Wan, B. Kan, Y. Wang, Y. Zhang, Q. Zhang, Y. Zuo, X. Yang and Y. Chen, *J. Mater. Chem. A*, 2015, **3**, 16679–16687; (b) Z. Ma, W. Sun, S. Himmelberger, K. Vandewal, Z. Tang, J. Bergqvist, A. Salleo, J. W. Andreasen, O. Inganäs, M. R. Andersson, C. Müller, F. Zhang and E. Wang, *Energy Environ. Sci.*, 2014, **7**, 361-369.

13 (a) S. Liu, X. Bao, W. Li, K. Wu, G. Xie, R. Yang and C. Yang, *Macromolecules* 2015, **48**, 2948−2957; (b) Q. Zhang, Y. Wang, B. Kan, X. Wan, F. Liu, W. Ni, H. Feng, T. P. Russell and Y. Chen, *Chem. Commun.* 2015, **51**, 15268-15271; (c) X. Guo, M. Zhang, L. Huo, F. Xu, Y.Wu, J. Hou, *J. Mater. Chem.* 2012, **22**, 21024−21031; (d) J. C. Bijleved, R. A. M. Verstrijden, M. M. Wienk and R. J. Janssen, *J. Mater. Chem.* 2011, **21**, 9224.

14 Q.-R. Yin, J.-S. Miao, Z. Wu, Z.-F. Chang, J.-L. Wang, H.-B. Wu and Y. Cao, *J. Mater. Chem. A.* 2015, **3**, 11575-11586.

15 W. Zhang, J. Smith, S. E. Watkins, R. Gysel, M. McGehee, A. Salleo, J. Kirkpatrick, S. Ashraf, T. Anthopoulos, M. Heeney and I. McCulloch, *J. Am. Chem. Soc.* 2010, **132**, 11437-11439.

16 M. J. Frisch, G. W. Trucks, H. B. Schlegel, G. E. Scuseria, M. A. Robb, J. R. Cheeseman, G. Scalmani, V. Barone, B. Mennucci, G. A. Petersson, H. Nakatsuji, M. Caricato, X. Li, H. P. Hratchian, A. F. Izmaylov, J. Bloino, G. Zheng, J. L.Sonnenberg, M. Hada, M. Ehara, K. Toyota, R. Fukuda, J. Hasegawa, M. Ishida, T. Nakajima, Y. Honda, O. Kitao, H. Nakai, T. Vreven, J. A. Montgomery, J. E. Peralta, F. Ogliaro, M. Bearpark, J. J. Heyd, E. Brothers, K. N. Kudin, V. N. Staroverov, R. Kobayashi, J. Normand, K. Raghavachari, A. Rendell, J. C. Burant, S. S. Iyengar, J. Tomasi, M. Cossi, N. Rega, N. J. Millam, M. Klene, J. E. Knox, J. B. Cross, V. Bakken, C. Adamo, J. Jaramillo, R. Gomperts, R. E. Stratmann, O. Yazyev, A. J. Austin, R. Cammi, C. Pomelli, J. W. Ochterski, R. L. Martin, K. Morokuma, V. G. Zakrzewski, G. A. Voth, P. Salvador, P.; J. J. Dannenberg, S. Dapprich, A. D. Daniels, Ö. Farkas, J. B. Foresman, J. V. Ortiz, J. Cioslowski, D. J. Fox and D. J. Gaussian, Wallingford CT, **2009**.

17 (a) G. L. Schulz, M. Löbert, I. Ata, M. Urdanpilleta, M. Lindén, A. Mishra and P. Bäuerle, *J. Mater. Chem. A* 2015, **3**, 13738-13748; (b)K. Sun, Z. Xiao, E. Hanssen, M. F. G. Klein, H. H Dam, M. Pfaff, D. Gerthsen, W. W. H. Wong and D. J. Jones, *J. Mater. Chem. A* 2014, **2**, 9048-9054.

18 (a) C. M. Proctor, J. A. Love and T.-Q. Nguyen, *Adv. Mater.,* 2014, **26**, 5957-5961; (b) A. Bull, L. S. C. Pingree, S. A. Jenekhe, D. S. Ginger and C. L. Luscombe, *ACS Nano.*, 2009, 3, 627-636.

19 (a) Shuttle, C. G.; Treat, N. D.; Douglas, J. D.; Fréchet, J. M. J.; Chabinyc, M. L. *Adv. Energy. Mater.*, 2012, **2**, 111-119; (b) Maurano, A.; Shuttle, C. G.; Hamilton, R.; Ballantyne, A. M.; Nelson, J.; Zhang, W.; Heeney, M.; Durrant, J. R. *J. Phys. Chem. C*, 2011, **115**,5947-5957.

TOC:

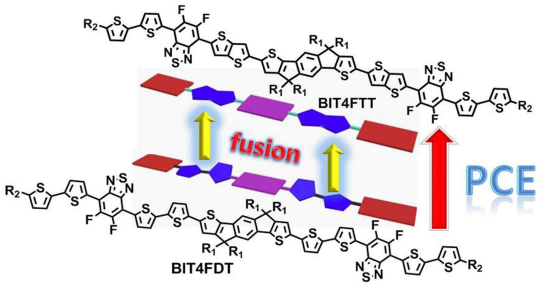

Small molecules **BIT4FDT** and **BIT4FTT** were synthesized, and **BIT4FTT** containing fused two thiophene rings as the π-conjugated spacers exhibited better PCE of ca. 7.6%.